14th International Conference on Applications of Statistics and Probability in Civil Engineering, ICASP14
Dublin, Ireland, July 9-13, 2023

Damage detection and model updating of a steel frame structure by measured strain and acceleration for improving seismic performance assessment

Taro Yaoyama
Project Assistant Professor, Dept. of Architecture, Univ. of Tokyo, Tokyo, Japan

Tatsuya Itoi
Associate Professor, Dept. of Architecture, Univ. of Tokyo, Tokyo, Japan

Jun Iyama
Associate Professor, Dept. of Architecture, Univ. of Tokyo, Tokyo, Japan

ABSTRACT: This paper presents a methodology for integrating acceleration and strain measurement to localize structural damage and to update the analytical model of a steel structure, which is validated by a vibration experiment on a full-scale, one-story, one-bay by one-bay moment-resisting steel frame, where damage of column bases was simulated by loosening the anchor bolts. The results demonstrated that model updating based on identified bending-moment mode shapes explicitly provides the rotational stiffness of the column bases and successfully identifies the localized stiffness reduction.

1. INTRODUCTION

Risk-informed decision making on various actions for existing civil structures (such as repair, retrofit, and business continuity planning) requires a quantitative assessment of seismic performance for future possible earthquakes that can effectively deal with and reduce uncertainties. Predicting responses to earthquake ground motions based on dynamic analysis serves this purpose, but there generally exists a large discrepancy between an analytical model and the counterpart real structure mainly due to: (a) modelling error and over-idealization; (b) variation in construction accuracy; (c) retrofit or conversion after construction; (d) degradation due to aging; (e) damages induced by disturbances like earthquakes. Vibration-based methodologies for model updating and damage detection thus play a significant role for improving simulation-based response prediction and performance assessment.

Most existing vibration-based methods for model updating and/or structural health monitoring (SHM) used modal properties such as natural frequencies, damping ratios, and displacement mode shapes that are identified from measured acceleration responses. Other studies used a dynamic strain measurement because of its higher sensitivity to local damages of structural elements (e.g., the buckling or fracture of a beam-column connection in a steel structure). They used, for example, strain-based frequency response functions (Esfandiari et al. (2010)), strain-based power spectral density (Pedram et al. (2016)), and strain mode shapes (Singh et al. (2018)), demonstrating that strain measurement allows accurate, sensitive, and informative model updating and damage localization. A few studies, furthermore, jointly used both acceleration and strain measurement for SHM purposes. Lee et al. (2013) used frequency response functions in terms of both quantities for localizing damage in a simply supported beam. Iyama et al. (2021) used both accelerometers and strain gauges for estimating the stiffness and stress distributed in an actual building. Integration of acceleration and strain allows us to relate modal displacements to the

corresponding stress and thus is expected to directly provide a better understanding of local stiffness reduction.

This paper presents a methodology for integrating acceleration and strain measurement to localize structural damage and to update the analytical model of a steel structure. The methodology consists of subspace state space system identification and bending-moment-based model updating and is validated by a full-scale vibration experiment on a moment-resisting steel frame, where structural damages were simulated by loosening the anchor bolts of column bases. The following part formulates a procedure for identifying modal properties including bending-moment mode shapes (Section 2), describes details of a full-scale vibration experiment (Section 3), and demonstrates using the experimental data that bending-moment-based model updating successfully quantifies the localized stiffness reduction (section 4).

2. IDENTIFICATION METHOD

2.1. Output-only system identification

To deal with free vibration responses to unknown inputs, let us consider an *output-only* system identification: Subspace State Space System Identification based on Stochastic Realization Theory (Katayama (2005)), hereafter termed *4SID-SRT*. In a stochastic realization theory, the following state space model is considered:

$$\mathbf{x}(t+1) = \mathbf{A}\mathbf{x}(t) + \mathbf{w}(t) \tag{1}$$

$$\mathbf{y}(t) = \mathbf{C}\mathbf{x}(t) + \mathbf{u}(t) \tag{2}$$

where $\mathbf{x} \in \mathbb{R}^n$ is the state vector, $\mathbf{y} \in \mathbb{R}^p$ is the output vector (observation), $\mathbf{w}(t) \in \mathbb{R}^n$ is the system noise vector, and $\mathbf{v}(t) \in \mathbb{R}^p$ is the observation noise vector. $\mathbf{A} \in \mathbb{R}^{n\times n}$ and $\mathbf{C} \in \mathbb{R}^{p\times n}$ are constant and hereafter called *system matrices*. The goal of 4SID-SRT is to obtain these system matrices.

According to Katayama (2005), the matrices $\mathbf{A}$ and $\mathbf{C}$ can be obtained in the following procedure. First, from observations $\{\mathbf{y}(t) \mid t = 0, ..., N+2k-2\}$, construct the block Teoplitz matrix $\mathbf{Y}_\mathrm{p} \in \mathbb{R}^{kp\times N}$ (corresponding to 'past' data) and the block Hankel matrix $\mathbf{Y}_\mathrm{f} \in \mathbb{R}^{kp\times N}$ (corresponding to 'future' data):

$$\mathbf{Y}_\mathrm{p} = \begin{bmatrix} \mathbf{y}(k-1) & \mathbf{y}(k) & \cdots & \mathbf{y}(N+k-2) \\ \mathbf{y}(k-2) & \mathbf{y}(k-1) & \cdots & \mathbf{y}(N+k-3) \\ \vdots & \vdots & & \vdots \\ \mathbf{y}(0) & \mathbf{y}(1) & \cdots & \mathbf{y}(N-1) \end{bmatrix} \tag{3}$$

$$\mathbf{Y}_\mathrm{f} = \begin{bmatrix} \mathbf{y}(k) & \mathbf{y}(k+1) & \cdots & \mathbf{y}(k+N-1) \\ \mathbf{y}(k+1) & \mathbf{y}(k+2) & \cdots & \mathbf{y}(k+N) \\ \vdots & \vdots & & \vdots \\ \mathbf{y}(2k-1) & \mathbf{y}(2k) & \cdots & \mathbf{y}(N+2k-2) \end{bmatrix} \tag{4}$$

Using these matrices, compute the Singular Value Decomposition (SVD) of the covariance matrix $\mathbf{S}_\mathrm{fp} = \mathbf{Y}_\mathrm{f}\mathbf{Y}_\mathrm{p}^\top/N$:

$$\mathbf{S}_\mathrm{fp} = \mathbf{U}\mathbf{S}\mathbf{V}^\top \tag{5}$$

where $\mathbf{U}, \mathbf{S}, \mathbf{V} \in \mathbb{R}^{kp\times kp}$, and $\mathbf{S}$ is a diagonal matrix whose elements are the singular values, i.e., $\mathbf{S} = \mathrm{diag}(\sigma_1, \sigma_2, ..., \sigma_{kp})$. Ignoring sufficiently small sigular values $\sigma_{n+1} > \sigma_{n+2} > ... > \sigma_{kp}$, compute the extended observability matrix $\mathbf{O} \in \mathbb{R}^{n\times n}$:

$$\mathbf{O} = \mathbf{U}_{1:n}\,\mathrm{diag}(\sqrt{\sigma_1}, ..., \sqrt{\sigma_n}) \tag{6}$$

where $\mathbf{U}_{1:n}$ denotes a matrix given by extracting the first to the n-th columns of $\mathbf{U}$. Finally, the matrices $\mathbf{A}$ and $\mathbf{C}$ are given by:

$$\mathbf{A} = {}_{1:(k-1)p}\mathbf{O}^\dagger\,{}_{1:(k-1)p}\mathbf{O} \tag{7}$$

$$\mathbf{C} = {}_{1:p}\mathbf{O} \tag{8}$$

where the superscript † represents the pseudo inverse, and ${}_{1:p}\mathbf{O}$ denotes a matrix given by extracting the first to the p-th rows of $\mathbf{O}$.

2.2. Modal parameter estimation

Using the system matrices $\mathbf{A}$ and $\mathbf{C}$, the modal parameters of natural frequencies ω_j, damping ratios ζ_j, and mode shapes $\mathbf{u}_j \in \mathbb{R}^p$ are given by the following relationships:

$$\omega_j = \frac{|\log\lambda_j|}{\Delta t} \tag{9}$$

$$\zeta_j = -\frac{\log|\lambda_j|}{|\log\lambda_j|} \tag{10}$$

$$\mathbf{u}_j = \mathbf{C}\mathbf{v}_j \tag{11}$$

Figure 1: The experimental model.

where λ_j and $\mathbf{v}_j \in \mathbb{R}^n$ are the j-th eigenvalue and eigenvector of $\mathbf{A}$, and Δt is the sampling period.

In implementing 4SID-SRT for modal parameter estimation, the number of system order n (i.e., the length of the system vector $\mathbf{x}$) and the number of block rows k are critical parameters that should be carefully adjusted. Specifically, n is related to the number of identified vibration modes. Successful 4SID-SRT gives the conjugate pairs of complex eigenvectors and thus, in a practical sense, results in $n/2$ vibration modes.

2.3. *Modal bending moments*

Using identified vibration modes both in terms of acceleration and strain, the following procedure provides the bending-moment mode shapes, or simply called *modal bending moments*, in a planar frame. First, the values of the strain mode shapes (or *modal strains*) at a cross-section are transformed into the modal bending moments as follows.

$$M_i = (\varepsilon_{i,\mathrm{lo}} - \varepsilon_{i,\mathrm{up}})EZ/2 \tag{12}$$

where M_i is the modal bending moment for the i-th mode, $\varepsilon_{i,\mathrm{lo}}, \varepsilon_{i,\mathrm{up}}$ are the modal strains for the i-th mode on the lower and upper sides of the section, and E and Z are the Young's modulus and the section modulus. Then, the *normalized modal bending moment* $\hat{M}_i$ is computed using the modal acceleration a_i on the top of the frame.

$$\hat{M}_i = M_i/(-a_i/\omega_i^2) \tag{13}$$

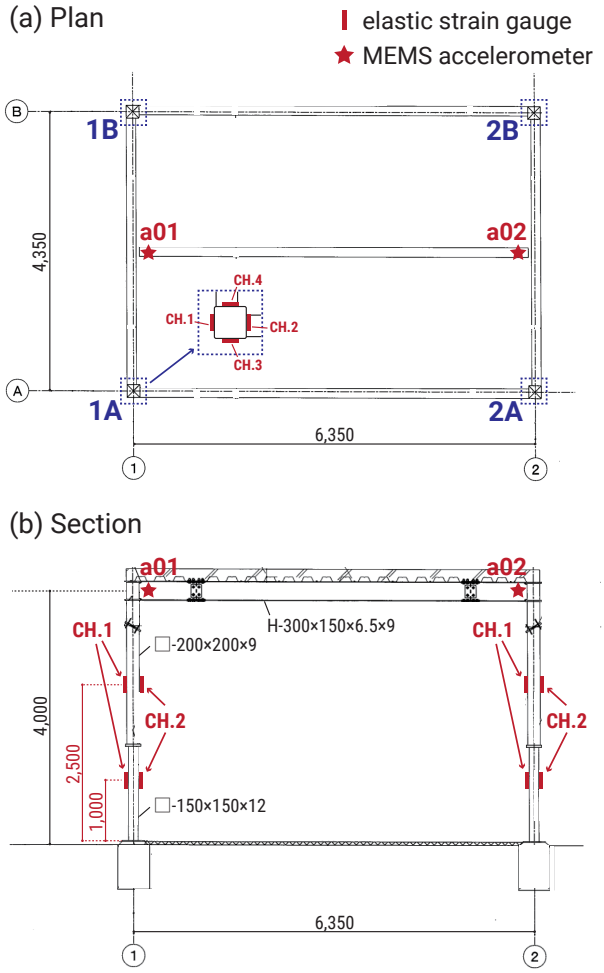

Figure 2: (a) Plan and (b) section (along B-axis) of the experimental model with sensor placement.

where ω_i is the i-th natrual angular frequency and thus $-a_i/\omega_i^2$ represents the i-th modal displacement of the top. Normalized modal bending moments $\{\hat{M}_i\}$ at several cross-sections give the distribution of bending moments in the frame when the lateral force is applied to induce a unit displacement of the top of the frame. Thus, integrating acceleration and strain directly provides the relationship between displacement and stress (i.e., stiffness) without knowledge of the mass, allowing a more informative model updating.

3. EXPERIMENTAL DATA

3.1. *Full-scale vibration experiment*

The experimental model, as shown in Figure 1, is a full-scale, one-story, one-bay by one-bay steel frame. The story height is 4,000 mm and the plan is 6,350 mm × 4,350 mm. Each of the four columns

Table 1: Considered cases in the experiment.

Case	Columns with loosened bolts
0	(intact)
1	1A
2	1A, 2A
3	1A, 2A, 1B
4	1A, 2A, 1B, 2B
5	all re-tightened

(whose locations are shown in Figure 2(a)) has two parts with different cross-section dimensions: the 1,500 mm lower part ($\square - 150 \times 150 \times 12$; $b/t = 12.5$) and the 2,600 mm upper part ($\square - 200 \times 200 \times 9$; $b/t = 22.2$), both of which were manufactured using the material STKR400, which has the Young's modulus 205,000 N/mm^2; the yielding strength 245 N/mm^2; the maximum strength 400 N/mm^2.

As shown in Figure 2(b), two 3-axis MEMS accelerometers were installed on the top of the test structure. Elastic strain gauges were also attached to all four sides of two sections of each column (one section at the upper part and the other at the lower part). The wireless sensor data is acquired through Rasberry Pi units. In total, 4-component acceleration response (two lateral components for each sensor) and 32-component strain response (eight components for each column) are used for system identification.

By manually exciting the structure in the longer-span direction, free vibration responses were measured for six different cases, Case 0–5 (listed in Table 1). The first case (Case 0) represents the initial intact state. In the second case (Case 1), the anchor bolts of the base of column 1A were loosened to simulate its stiffness reduction; in the following three cases (Case 2–4), those of the other three columns (2A, 1B, 2B) were loosened one by one. In the last case (Case 5), then, the anchor bolts of all column bases were re-tightened and an intact state was simulated again.

3.2. *Preprocessing data*

Time synchronization of measured signals was performed based on linear interpolation using timestamps of each unit. This was firstly performed

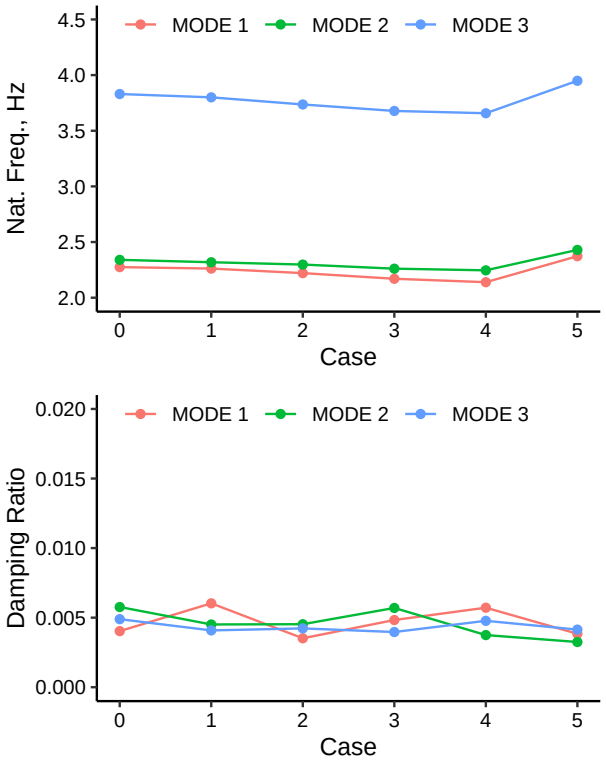

Figure 3: Identified natural frequencies and damping ratios for all cases.

individually for the strain gauges and accelerometers because of different sampling rates (87 Hz and 125 Hz, respectively). A cosine-tapered bandpass filter was then used to reduce noise in the low-frequency (below 1 Hz) and high-frequency (above 10 Hz) bands. Downsampling based on linear interpolation was finally performed so that all signals including strain and acceleration responses are synchronized and have the same sampling period $\Delta t = 0.046s$.

4. RESULTS

4.1. *Modal identification*

System identification based on 4SID-SRT is performed for each case, jointly using strain and acceleration responses. The number of system order is set as $n = 6$ based on preliminary examinations, and therefore practically three vibration modes, hereafter termed mode 1–3, are obtained. The number of block rows is set as $k = 30$. The time window (and data length N) used for identification is carefully determined for each case.

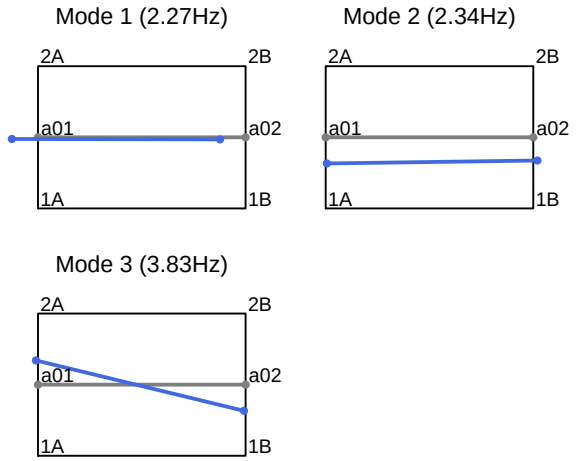

Figure 4: Identified displacement mode shapes (only real part) for mode 1–3 in Case 0.

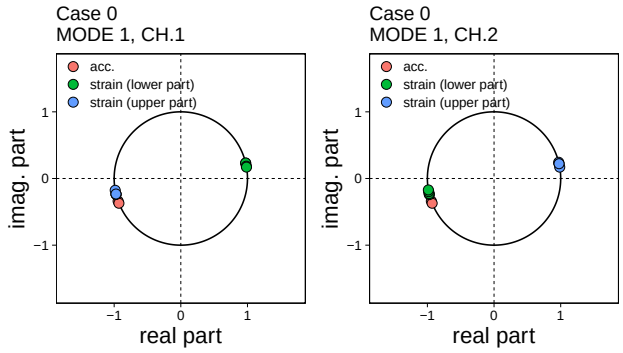

Figure 5: Phase of identified strain mode shapes.

Figure 3 shows the identified natural frequencies and damping ratios for the three vibration modes (mode 1–3) for all cases. The upper plot shows that, from Case 0 to Case 4, the natural frequencies of all modes gradually decrease; from Case 4 to Case 5, the natural frequencies recover and even exceed the initial level in Case 0. Loosening or tightening the anchor bolts thus substantially changes the vibration characteristics of the whole structure. The lower plot shows that the damping ratios are stably obtained for all cases and have similar values for all modes.

Figure 4 illustrates in a plan view the real part of the identified complex mode shapes of displacement at the locations of the two accelerometers for all modes in Case 0. This suggests that mode 1 and mode 2 respectively represent the translational modes in the longer-span and shorter-span directions, and mode 3 represents the planar rotational mode.

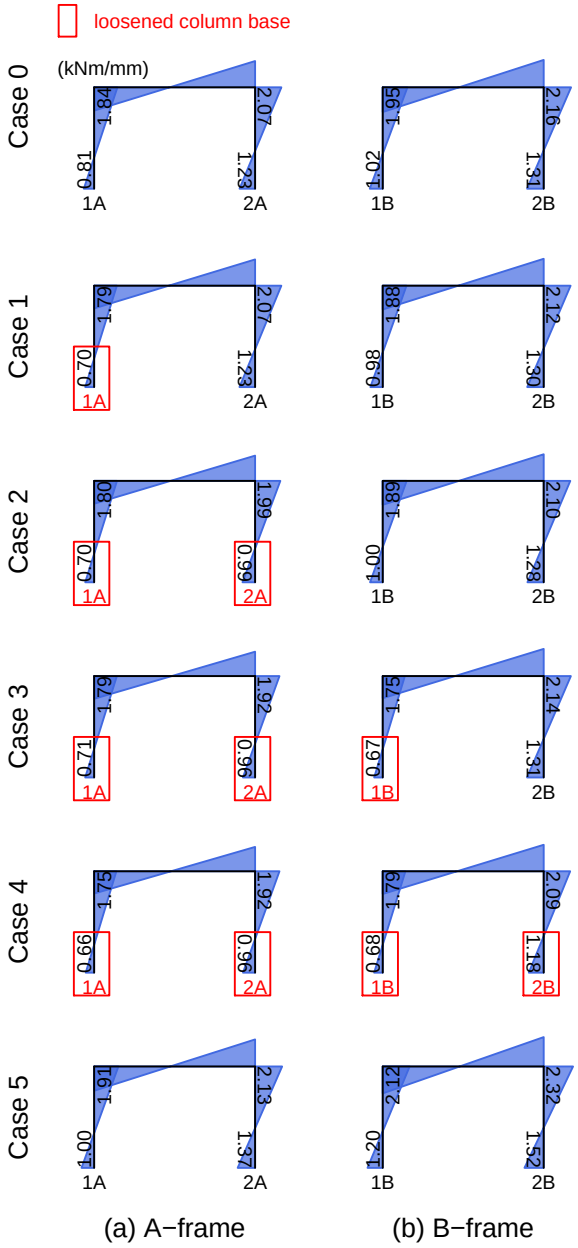

Figure 6: Identified bending moment diagrams of A- and B- frame for mode 1 for all cases.

Figure 5 shows, for mode 1 in Case 0, the argument (phase) of the identified complex mode shapes of strain at eight locations (for the upper and lower sensor gauges in each column) both for CH.1 and CH.2 (see Figure 2(b) for the definition of CH.1 and CH.2), and that of the corresponding mode shapes of acceleration in the longer-span direction for the

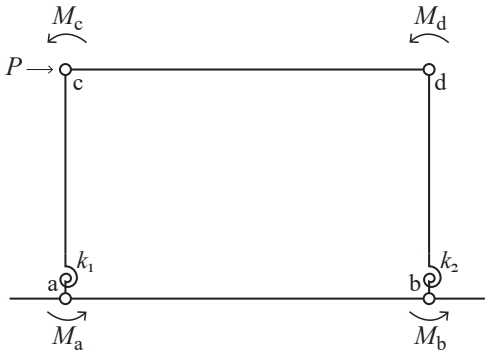

Figure 7: Structural model to update (illustrative).

two accelerometers. For the two channels, strain responses at the upper locations (represented by the blue dots) have a phase almost opposite to that of the lower locations (represented by the green dots). This suggests shear deformation of the columns, which corresponds to the above finding that mode 1 represents the longer-span direction translational mode.

Figure 6 shows the distribution of the normalized modal bending moments both in A-frame and B-frame identified for mode 1 in Case 0–5, for which the mean of modal acceleration between the two accelerometers is used as a_i in Eq. (13). These diagrams suggest that the subsequently induced stiffness reduction of columns 1A, 2A, 1B and 2B are clearly represented by the reduction of the bending moments of the corresponding bases; for example, the bending moment at the base of column 1A decreases by more than 10% from Case 0 to Case 1. This implies that the normalized bending-moment mode shapes have sufficient sensitivity for locating damages of the column bases.

4.2. *Model updating*

A moment-resisting frame with two rotational springs to represent semi-rigid column bases, as shown in Figure 7, is assumed for each frame (A- or B-frame) and updated to fit itself to the identified modal bending moments. The parameters to update are the stiffness of the rotational springs, k_1 and k_2. The mechanical and material properties of the other elements are fixed to the nominal values, but the Young's modulus of element c–d is set as ten times larger than its nominal value, assuming that

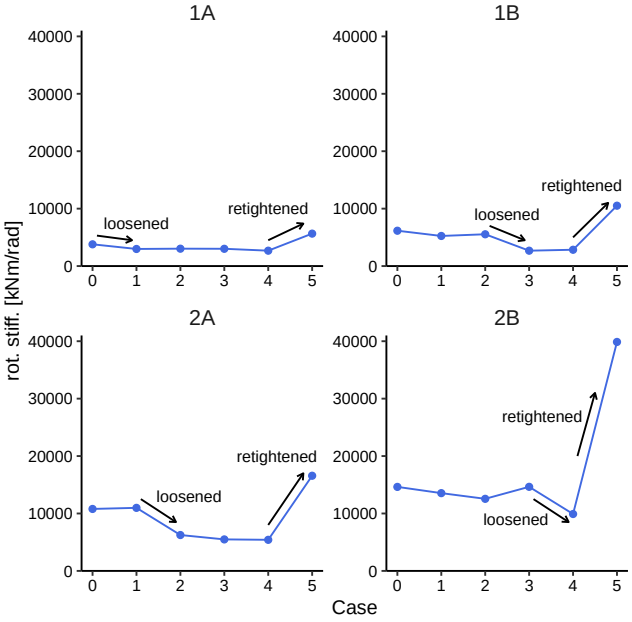

Figure 8: Updated rotational stiffness of column bases.

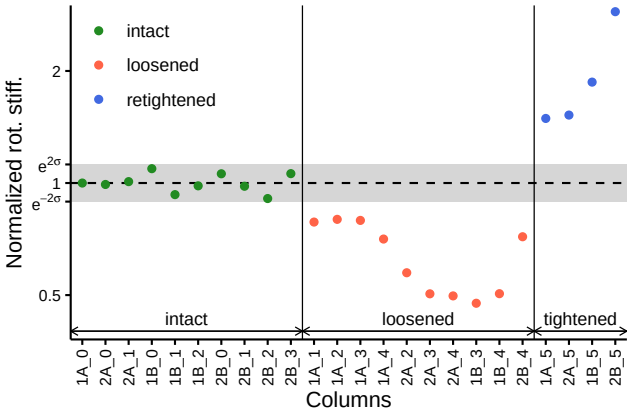

Figure 9: Normalized rotational stiffness for all cases and columns.

the beam is rigidified by its connection to the slab. The parameters are estimated by the least square method to minimize the residuals between the identified values of normalized modal bending moments at the nodes a, b, c, and d, and the simulated values when the lateral force P is applied at node c so that the lateral displacement of the node is 1 mm. Denoting the bending moments at the nodes a, b, c, d by M_a, M_b, M_c, M_d, the objective function is written as:

$$\min_{k_1,k_2} \sum_{j\in\{a,b,c,d\}} \left(M_j^{sid} - M_j^{sim}\right)^2 \qquad (14)$$

where the superscripts 'sid' and 'sim' represent identified and simulatated values. To solve this, the trust region reflective algorithm (Branch et al. (1999)) implemented in a Python package SciPy (Virtanen et al. (2020)) is used in this study.

Figure 8 shows for all cases the estimated rotational stiffness of all the four column bases. This figure captures the stiffness reduction of each column base induced by loosening the anchor bolts as well as the stiffness increase from Case 4 to Case 5 induced by re-tightening the bolts, demonstrating the applicability of our model updating method to structural damage localization.

To examine the sensitivity and robustness of the methodology, Figure 9 shows the normalized rotational stiffness for all column bases in all cases, which is computed as follows.

$$\bar{k}_{c,i} = k_{c,i} \Bigg/ \left(\prod_{j=0}^{N_c-1} k_{c,j} \right)^{1/N_c} \tag{15}$$

where $k_{c,i}$ is the rotational stiffness of column base $c \in \{1\mathrm{A}, 1\mathrm{B}, 2\mathrm{A}, 2\mathrm{B}\}$ in Case $i \in \{0, 1, ..., 5\}$, $\bar{k}_{c,i}$ is the corresponding normalized rotational stiffness, and N_c is the number of intact cases for column c (e.g., $N_{2\mathrm{A}} = 3$). The value $\bar{k}_{c,i}$ thus represents the ratio of the rotational stiffness of a column base to the geometric mean of the rotational stiffness values of the same column in all intact cases. The labels in the x-axis are given as 'column name'_'Case number' (e.g., '1A_0' represents the base of column 1A in Case 0). The shaded area is the range $[\mathrm{e}^{-2\sigma}, \mathrm{e}^{2\sigma}]$, where σ is the logarithmic standard deviation of the normalized rotational stiffness values of all column bases in all intact cases. All samples of the loosened and re-tightened column bases are respectively below and above this range. This suggests that the stiffness reduction (or increase) of column bases is more significant compared to the variability in the intact cases, which may be due to measurement noise, estimation error, and influence of other damaged elements, and that the bending-moment-based model updating allows sensitive and robust damage localization for steel column bases.

5. CONCLUSIONS

Towards development of a quantitative seismic performance assessment of structures combining monitoring, model updating, and response analysis, this paper has presented a methodology for integrating acceleration and strain measurement to localize structural damage and to update the analytical model of a steel structure. The proposed model updating procedure is based on bending-moment mode shapes that are obtained using subspace state space system identification applied to both acceleration and strain responses. To validate the methodology, a vibration experiment on a full-scale, one-story, one-bay by one-bay steel frame structure was conducted, where damage (stiffness reduction) of column bases was simulated by loosening the anchor bolts. The results demonstrated that bending-moment-based model updating using strain and acceleration responses explicitly provides the rotational stiffness of the column bases and successfully identifies the localized stiffness reduction.

6. ACKNOWLEDGEMENT

The dynamic loading test in this study was a part of collaborative research conducted by Prof. Satoshi Yamada and Prof. Tsuyoshi Seike at the University of Tokyo and supported by JSPS KAKENHI (Grant-in-Aid for Scientific Research(B)) Grant Number JP20H02293.

7. REFERENCES

Branch, M. A., Coleman, T. F., and Li, Y. (1999). "A subspace, interior, and conjugate gradient method for large-scale bound-constrained minimization problems." *SIAM Journal on Scientific Computing*, 21, 1–23.

Esfandiari, A., Sanayei, M., Bakhtiari-Nejad, F., and Rahai, A. (2010). "Finite element model updating using frequency response function of incomplete strain data." *AIAA Journal*, 48(7), 1420–1433.

Iyama, J., Chih-Chun, O., and Araki, K. (2021). "Bending moment distribution estimation of an actual steel building structure by microstrain measurement under small earthquakes." *Journal of Civil Structural Health Monitoring*, 11, 791–807.

Katayama, T. (2005). *Subspace methods for system identification*. Springer.

Lee, E.-T., Rahmatalla, S., and Eun, H.-C. (2013). "Damage detection by mixed measurements using accelerometers and strain gages." *Smart Materials and Structures*, 22, 075014.

Pedram, M., Esfandiari, A., and Khedmati, M. R. (2016). "Finite element model updating using strain-based power spectral density for damage detection." *Structural Control and Health Monitoring*, 23, 1314–1333.

Singh, M. P., Elbadawy, M. Z., and Bisht, S. S. (2018). "Dynamic strain response measurement-based damage identification in structural frames." *Structural Control and Health Monitoring*, 25, e2181.

Virtanen, P. et al. (2020). "SciPy 1.0: Fundamental Algorithms for Scientific Computing in Python." *Nature Methods*, 17, 261–272.